Focused Traveling Surface Acoustic Wave-Based Acoustofluidic Chip for Label-Free Cell Sorting

Jingxiang Deng[a,b], Yang Yang[c], Zixin Wang[d], Haiping Zhao[e], Hao Chen[a,b], Lingqian Zhang[a], Mingxiao Li[a], Yang Zhao[a*] and Chengjun Huang[a,b*]

[a]Institute of Microelectronics of the Chinese Academy of Sciences, Beijing 100029, China

[b]University of Chinese Academy of Sciences, Beijing 100049, China

[c]Department of Medicine, Brigham and Women's Hospital, Harvard Medical School, Boston, MA 02115, USA

[d]Department of Neurology, Xuanwu Hospital, Capital Medical University, Beijing, China

[e]Institute of Cerebrovascular Diseases Research, Xuanwu Hospital of Capital Medical University, 45 Changchun Street, Beijing, 100053, China.

E-mail addresses: zhaoyang@ime.ac.cn and huangchengjun@ime.ac.cn

Supplementary information

Supplementary Fig. 1

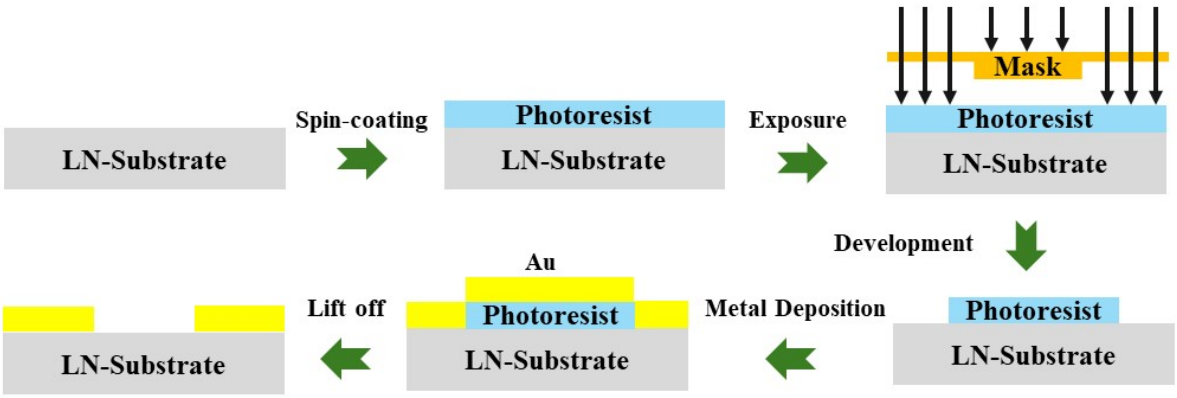

Fig. S1 Schematic of the fabrication process for the focused interdigital transducers (FIDTs). The process begins with uniformly spin-coating a layer of photoresist onto a 500 μm-thick lithium niobate ($LiNbO_3$) substrate. A photomask is then aligned and used to expose the photoresist, defining the desired pattern. Following exposure, the substrate is developed to remove the unexposed regions. A 100 nm-thick gold layer is subsequently deposited over the entire structure via magnetron sputtering. Finally, a lift-off process is performed to remove the excess metal, leaving behind the patterned gold FIDTs on the $LiNbO_3$ substrate.

Supplementary Fig. 2

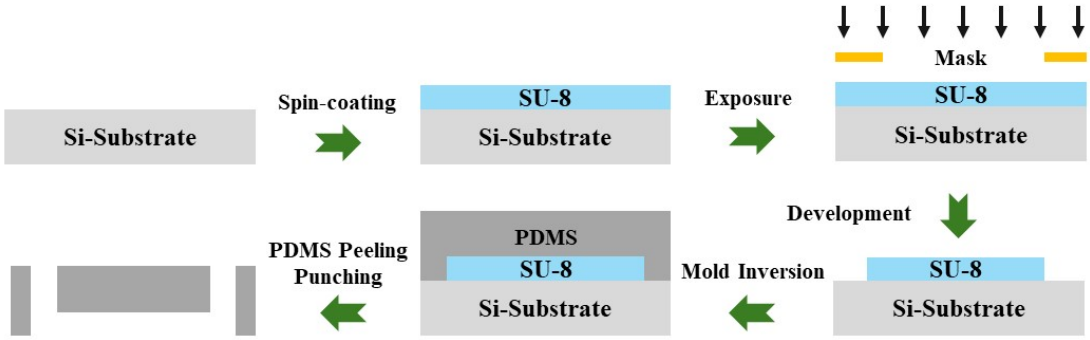

Fig. S2 Schematic of the microchannel mold fabrication process. The process begins with spin-coating a uniform layer of SU-8 negative photoresist onto a silicon wafer. A photomask is then aligned and brought into contact with the photoresist for UV exposure, transferring the microchannel pattern. After development, the resulting three-dimensional channel structures remain as raised features on the wafer surface, forming the master mold. Next, a mixture of polydimethylsiloxane (PDMS) prepolymer and curing agent is poured onto the master mold. Subsequently, it is thermally cured to solidify the PDMS. Finally, the cured PDMS slab is carefully peeled off from the silicon master, and inlet/outlet ports are punched to complete the fabrication of the microfluidic device used in the experiments.

Supplementary Fig. 3

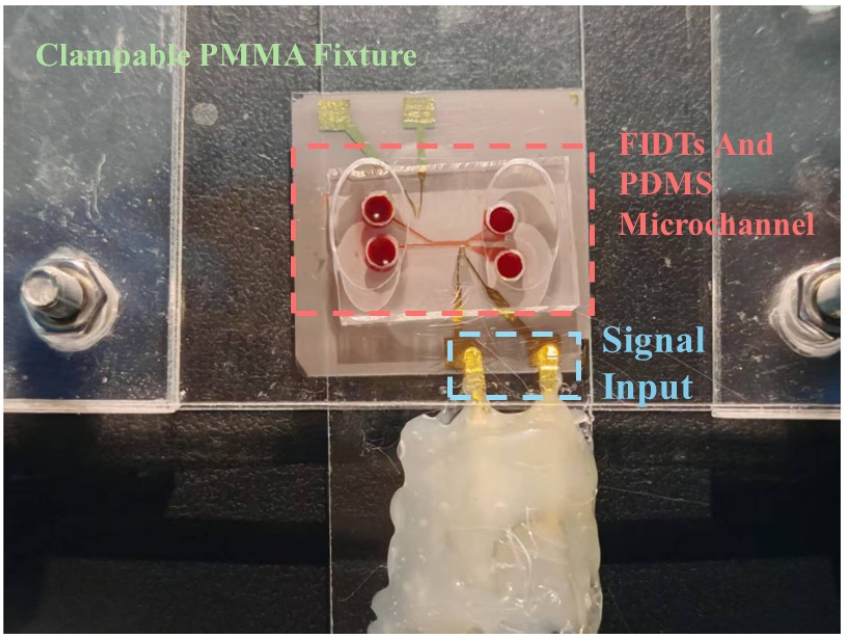

Fig. S3 Photograph of the custom-made PMMA clamping fixture. This fixture employs a dual-layer rectangular plate design to ensure precise alignment and robust, leak-free integration of the PDMS microchannel with the underlying focused interdigital transducers (FIDTs) on the $LiNbO_3$ substrate. Four corner screws are tightened to apply uniform pressure, securing the assembly and maintaining a hermetic seal throughout the acoustofluidic experiments.

Supplementary Fig. 4

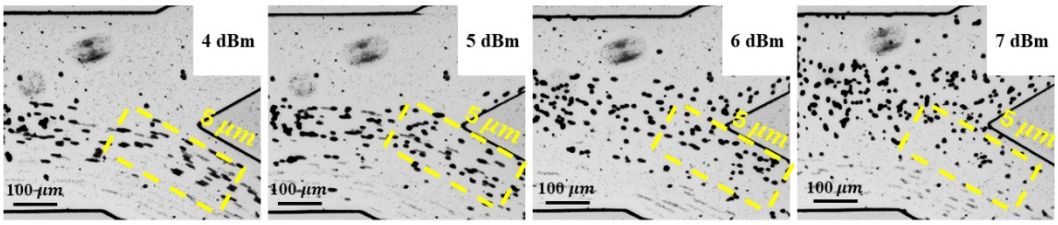

Fig. S4 Trajectory images of PS beads at FTSAW input powers ranging from 4 to 7 dBm. At 4 dBm, the 5 μm beads exhibited a focused trajectory but remained within the lower stream, following the fluid flow to the waste outlet. As the input power increased, the trajectories systematically shifted upward. At 7 dBm, the majority of the 5 μm beads were deflected significantly by the acoustic radiation force and directed toward the target outlet. However, a small fraction continued to follow the waste outlet stream, indicating that the acoustic force at this power was near, but not fully above, the critical threshold for complete sorting.

Supplementary Fig. 5

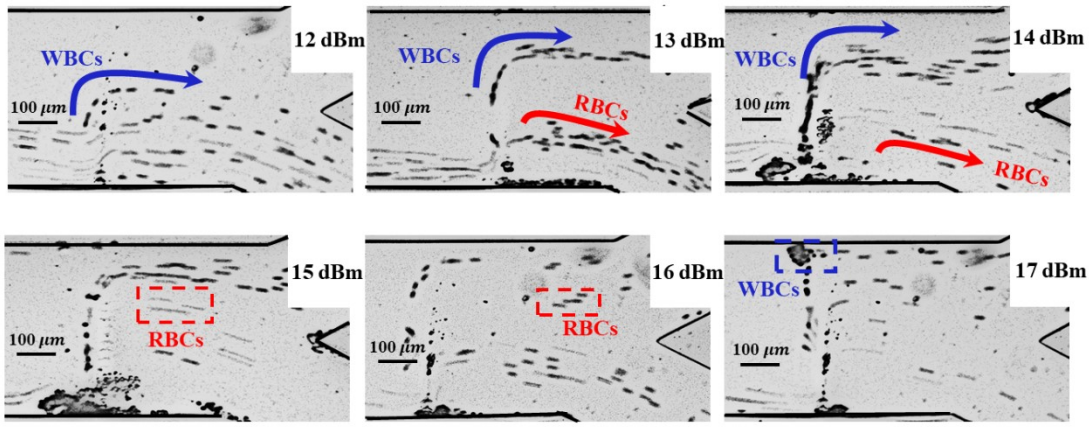

Fig. S5 Cellular trajectory images at FTSAW input powers from 12 to 17 dBm. At 12 dBm, white blood cells (WBCs) first exhibited trajectory focusing. With increasing input power, the lateral displacement of WBCs increased while their trajectories remained relatively stable. However, a fraction of red blood cells (RBCs) from the upper stream were also progressively deflected toward the target outlet by the stronger acoustic radiation force, thereby contaminating the purity of the collected WBCs. When the input power reached 17 dBm, the WBCs were driven to the upper channel wall, resulting in pronounced cell aggregation.

Supplementary Fig. 6

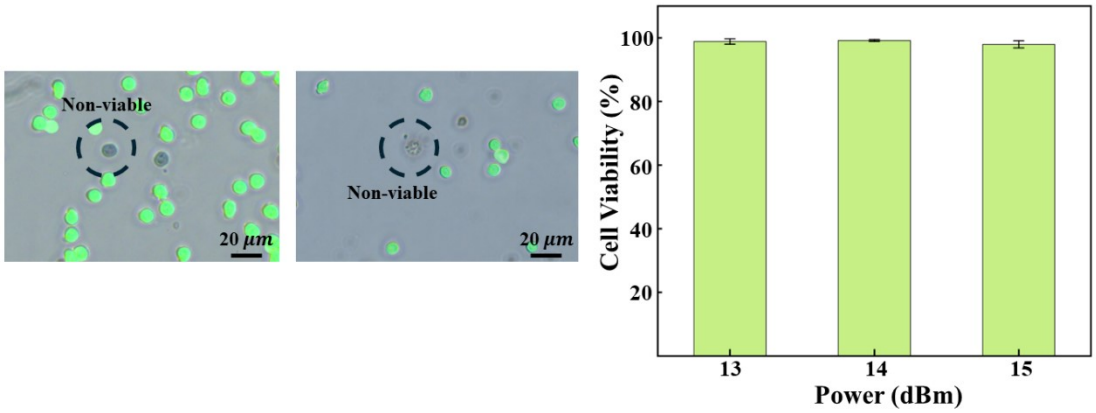

Fig. S6 Cell viability. The viability of the collected target cells was assessed by classifying non-fluorescent (Calcein negative) white blood cells (WBCs) and cells with significantly altered morphology as non-viable. The overall cell viability was maintained at ~98% across all experimental conditions.